Article

Bioinspired Heterogeneous Ion Pump Membranes: Unidirectional Selective Pumping and Controllable Gating Properties Stemming from Asymmetric Ionic Group Distribution

Zhen Zhang, Pei Li, Xiang-Yu Kong, Ganhua Xie, Yongchao Qian, Ziqi Wang, Ye Tian, Liping Wen, and Lei Jiang

J. Am. Chem. Soc., **Just Accepted Manuscript** • DOI: 10.1021/jacs.7b11472 • Publication Date (Web): 20 Dec 2017

Bioinspired Heterogeneous Ion Pump Membranes: Unidirectional Selective Pumping and Controllable Gating Properties Stemming from Asymmetric Ionic Group Distribution

Zhen Zhang,[†,||] Pei Li,[§] Xiang-Yu Kong,[‡] Ganhua Xie,[†,||] Yongchao Qian,[‡] Ziqi Wang,[‡,||] Ye Tian,[*,†] Liping Wen,[*,‡,§,||] and Lei Jiang[*,‡,§,||]

[†]Beijing National Laboratory for Molecular Sciences (BNLMS), Key Laboratory of Green Printing, Institute of Chemistry, Chinese Academy of Sciences, Beijing 100190, P. R. China

[‡]Key Laboratory of Bio-inspired Materials and Interfacial Science, Technical Institute of Physics and Chemistry, Chinese Academy of Sciences, Beijing 100190, P. R. China

[§]School of Chemistry and Environment, Beihang University, Beijing 100191, P. R. China

[||]University of Chinese Academy of Sciences, Beijing 100049, P. R. China

ABSTRACT: The creation of artificial solid-state ion pump that mimics the delicate ion transport behaviors of biological protein-based ion pump is drawing more and more research attention due to its potential applications in energy conversion, biosensor, and desalination. However, the reported bioinspired double-gated ion pump systems are generally very primary, and can only realize non-selective ion pumping functions with no directionality and uncontrollable ion gating functions, which are far from their biological counterparts. To make the bioinspired device "smart" in real sense, the implementation of high-level selectivity and directionality in the ion pumping process, meanwhile achieving great controllability in the ion gating process is a necessity. Here, we developed a bioinspired heterogeneous ion pump membrane by combining block copolymer membrane sacrificial coating and plasma grafting technique. The system behaves unidirectional selective ion pumping and controllable ion gating properties. The introduction of asymmetric ionic group distribution is the key reason for its novel transport behaviors. Such a heterogeneous ion pump could not only provide a basic platform that potentially sparks further efforts to simulate the smart ion transport processes in living bodies, but also promote the application of artificial nanofluidic devices in energy conversion, water treatment, and biosensing.

INTRODUCTION

Precisely controllable transport of various ions into and out of cells and organelles through asymmetric ion channels and ion pumps mediate processes as disparate as volume regulation, muscle contraction, and signal transmission, etc.[1-5] Different from the biological ion channel in which the ion movements are governed by one single gate, ion pumps have two separate intelligent gates located separately at two ends of the ion pathway, which lays the foundation for its delicate ion transport functions.[6] As shown in **Figure 1a**, the two gates can open and close alternately in response to external stimuli, allowing the chosen ions to enter the pore cavity from one side of the plasma membrane while one of the gates is open, and then to leave at the other side while the other gate is open, after the first gate has absolutely shut. This process is commonly highly ion-selective and ubiquitous in biological ion pumps such as Na^+/Ca^{2+} exchangers.[7] It can also function as an ion channel (i.e. pump–channel in Na^+/K^+ ATPase,[8] for example) that conducts substantial dissipative fluxes controllably if both gates open or close simultaneously. Furthermore, the biological system such as Ca^{2+}ATPase[9] or Na^+/K^+ ATPase[10] also evolves a fail-safe mechanism to prevent the communication breakdown between the two gates, in which both gates first close, occluding the chosen ions inside the pore cavity before the second gate opens to release them.

Inspired from nature, the integration of two separate gates, asymmetric geometry, and a reserving space of ion storage serves as essential requirements to build artificial analogs of the biological ion pump.[11] During the past few years, various ion transport properties of biological ion channels have been artificially realized using solid state nanochannels.[12-19] However, the investigations of bioinspired ion pumps are still in the early stage.[20-23] In 2013, Zhang *et al.* reported the first double-gated artificial ion pump based on a symmetric cigar-shaped nanochannel.[24] Although this primary system can realize the basic transport functions of biological ion pump, the ion pumping process do not exhibit selectivity and directionality, and the ion transport processes do not have controllability because of the difficulty in tuning the comparative complex ion pumping mechanisms governed by the two separate gates. In order to mimic the delicate ion

transport phenomena of the biological counterpart in depth and broaden the future application scenarios of the artificial counterpart, the implementation of high-level selectivity and directionality in the ion pumping process, meanwhile achieving great controllability in the ion gating process is a necessity, which can make the artificial device "smart" in real sense.[6,25,26] Recently, the researches concerning heterogeneous nanochannel membrane that is fabricated via the hybridization of two homogeneous membranes with different functionality are just emerging.[27,28] The heterogeneous nanochannel system with multilevel asymmetry, tunable structure, and superior ionic rectification is considered to be an excellent candidate that can integrate the unidirectional ion transport in a highly selective manner.[29-31]

Here we demonstrate an artificial heterogeneous ion pump membrane with unidirectional selective ion pumping and controllable ion gating properties. The hybrid membrane is prepared by coating a block copolymer (BCP) membrane, polystyrene-*b*-poly(4-vinylpyridine) (PS-*b*-P4VP), onto the large opening side of a track-etched polyethylene terephthalate (PET) membrane with conical nanochannels, followed by chemically grafting poly(acrylic acid) (PAA) brushes at the small opening side using plasma technique. The P4VP chains inside the pores of BCP membrane and the PAA brushes serve as two separate and opposite pH-responsive functional gates. This hybrid membrane can well reproduce the three transport functions of the biological ion pump through varying pH stimuli. Importantly, as an alternating gates ion pump, the system can selectively transport anion flux from the BCP membrane side to the small opening side with high-level selectivity and directionality. The PET channel with asymmetric geometry not only serves as a reserving space, but also introduces asymmetric ionic group distribution to the system, which is the key reason for this unidirectional ion pumping phenomenon. Also, benefiting from the feasibility and accuracy in tuning the diameter of the large openings of the PET nanochannels, which will change the exposed pore amount of BCP membrane facing the large opening of PET membrane, the gating behaviors can be precisely controlled. The system can also work well under a concentration gradient. Such a heterogeneous ion pump system could not only provide a basic platform that potentially sparks further efforts to simulate the smart ion transport processes in living bodies, but also promote the application of artificial nanofluidic devices in energy conversion, water treatment, and biosensing.[32-39]

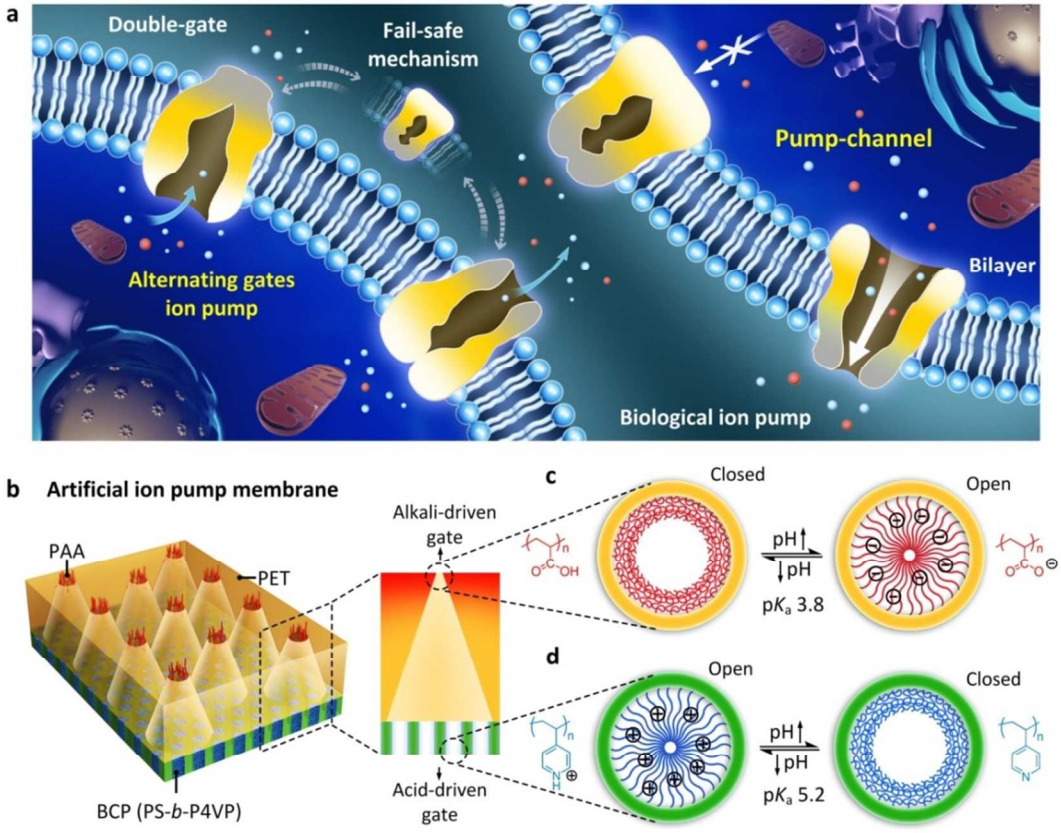

Figure 1. Bioinspired multifunctional heterogeneous ion pump membranes. (a) Generic model of the biological asymmetric ion pump with three unique ion transport features implemented by two separate intelligent gates located separately at two ends of the pathway. (b) Schematic of the heterogeneous ion pump membrane. (c) The PAA brushes at the tip of PET membrane can undergo pH responsive conformational changes from the closed state to the open state. (d) Oppositely, the P4VP chains inside the pores of BCP membrane can undergo pH responsive conformational changes from the open state to the closed state.

RESULTS AND DISCUSSION

Figure 1b shows the schematic of the heterogeneous ion pump membrane. Asymmetric conical nanochannels embedded within a PET membrane are prepared by the well-developed track-etching technique (pore density~ 10^6 pores/cm^2).[40] The chemical etching process will create mobile carboxyl groups on the channel walls.[41] The small opening of the conical nanochannel is called the tip and the large opening is called the base. Diameter of the bases can be controlled using a solvent shaping method by adopting mixture of ethanol and water as the etching solution (Supporting Text 1 and Figure S1-S2), meanwhile maintaining size of the tips relatively constant (9~15 nm).[42] Notably, the PET membrane actually exhibits a non-uniform pore distribution owing to the uncontrollable ion-tracks formation process. In order to fabricate the hybrid membrane, the BCP membrane is cast onto the PET substrate by a spin-coating method. To prevent the penetration of BCP solution, a sacrificial layer of poly(sodium-p-styrenesulfonate) (PSS) was filled into the channel cavity beforehand and can be completely dissolved afterwards (Supporting Text 2 and Figure S3-S4). Then the tip of PET substrate is grafted with PAA brushes using plasma grafting technique (Experimental Section).[24,43] The BCP membrane with a thickness about 1.2 μm exhibits an asymmetric structure composed of a thin layer of hexagonally packed pores (pore size~ 16 nm; pore density~ 6×10^{10} pore/cm^2) atop a disordered layer (Figure S5-S6).[44] The pores (blue part) embedded within the PS matrix (green part) are filled with P4VP chains containing pyridine groups (pK_a~ 5.2);[45] the polymer chains will exhibit swollen, charged, and hydrophilic state when the pH value was less than the pK_a; otherwise, they will exhibit collapsed, uncharged, and hydrophobic state.[46,47] Oppositely, the PAA brushes at the tip containing carboxyl groups (pK_a~ 3.8) can undergo pH-responsive conformational changes from collapsed, uncharged, and hydrophobic state to swollen, charged, and hydrophilic state upon increasing the pH beyond 3.8 (**Figure 1c, d**). At first glance, the conformation change of polymer chains from the collapsed state to swollen state will result in a decrease in the pore size and thus a closed state of the nanochannel. However, in our case of the polymer filled nanochannel, the joint effect of charge and wettability plays a more prominent role.[48] The changes into hydrophilic and charged state will "largen" the effective pore size, resulting in an open state. On the contrary, the changes into hydrophobic and neutral state will "shrink" the effective pore size, resulting in a closed state. The two polymer gates, PAA and P4VP, can act as gatekeepers managing and constraining the flow of ion species with four types of states, namely, open/ closed, closed/ open, open/ open, and closed/ closed states, which can be realized by successively stimulating the two sides of the membrane using alkaline/ alkaline, acidic/ acidic, alkaline / acidic, and acidic / alkaline conditions. Notably, the asymmetric geometry of PET channel will contribute to asymmetric group distribution on the two sides. As a result, the effect of P4VP gate on the ion transport is more remarkable than that of the PAA gate due to the high pore density of BCP membrane and large positive charge density of the P4VP chains.[49,50]

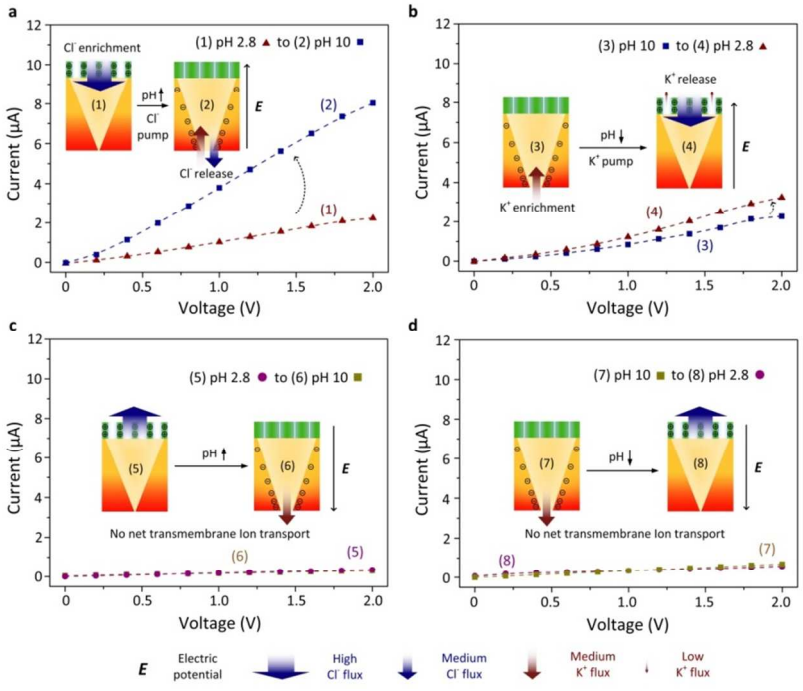

Figure 2. Unidirectional anion-selective alternating gates ion pump. (a, b) *I-V* curves of the heterogeneous membrane recorded in 0.1 M KCl under positive bias upon increasing the pH from 2.8 to 10 (a), and reversely decreasing pH from 10 to 2.8 (b). (c, d) *I-V* curves of the heterogeneous membrane recorded in 0.1 M KCl under negative bias upon increasing the pH from 2.8 to 10 (c), and reversely decreasing pH from 10 to 2.8 (d). In all conditions, the base of the PET membrane is approximately 1 μm in diameter. The insets show the mechanism of the unidirectional selective ion pump process.

The alternating gates ion pump with high-level selectivity and directionality can be realized by alternately opening the two polymer gates under symmetric pH stimuli. Representative current–voltage (*I-V*) responses (Experimental Section and Figure S7) for the heterogeneous membrane are shown in **Figure 2**. The cathode is placed in the tip side. The base of the PET membrane is approximately 1 μm in diameter. Upon increasing the pH from 2.8 to 10, pumping phenomenon is observed evidenced by an increase of the current recorded at 2 V from 2.2 μA to 8.0 μA (**Figure 2a**). At pH 2.8, the PVP chains inside the pores of BCP membrane are in the swollen, charged, and hydrophilic state (open state), while the PAA brushes are in the collapsed, noncharged, and hydrophobic state (closed state). Due to the high pore density of BCP membrane and large positive charge density of the P4VP chains, the opening of the P4VP gates at pH 2.8 will allow large amounts of counter-ion (Cl^-) to move into and negligible amounts of co-ion (K^+) to move out of the PET cavity (**Figure 2a**, inset).[51] The stored Cl^- will cause a high concentration gradient between the pore cavity and the solution phase of the PAA side, while the PAA gate at the tip is closed and blocks the ion transport, inducing a low ion current state. Increasing the pH to about 10 will open the PAA gate, and the medium amounts of K^+ will first enter into the cavity due to the matched charge polarity. At the same time, the high concentration gradient of Cl^- in the tip side will overcome the unfavorable electrostatic effect of the PAA brushes, and the Cl^- stored in the cavity will be released into the solution. Net Cl^- is transported across the membrane from the solution of base side to the solution of tip side with this pH rising process, resulting in a largely increased ion current. This pumping process is largely hindered in high concentration electrolyte due to the weakened electrostatic interaction (Figure S8). It is worth to mention that the energy source to drive ions into and out of the nanochannel is the external applied voltage, not the adenosine triphosphate in living systems.

Interestingly, the situation is completely different when we conduct this process in a reverse manner. As shown in **Figure 2b**, when we change the pH value reversely from 10 to 2.8, the current recorded at 2 V only slightly increases from 2.3 μA to 3.2 μA. At pH 10, the PAA gate is first open. Because of the low pore density of PET membrane, medium amounts of counter-ion (K^+) and negligible amounts of co-ion (Cl^-) will move into and out of the PET cavity, respectively. As discussed before, the enriched K^+ will also cause a concentration gradient between the pore cavity and the solution phase of the BCP side.[52] The ion transport is blocked by the closed P4VP gates and a low ion current is observed. After opening the P4VP gates by decreasing the pH value to 2.8, large amounts of Cl^- will first enter into the cavity. In this case, it worthy to note that the electrostatic screening effect of the positively charged P4VP chains to the enriched K^+ is much stronger than that of the negatively charged PAA chains to the enriched Cl^- in the Cl^- release process of Figure 2a due to the higher pore density and larger positive charge density of BCP membrane.[49,50] Only small amounts of the stored K^+ will be released and thus the net transmembrane transportation of K^+ is very small, accompanied by a slightly increased ion current. As an alternating gates ion pump, the system can selectively transport higher Cl^- flux than K^+ flux across the membrane.

If we reverse the direction of the driving force, the selective ion pumping phenomenon will disappear, indicating that the ion transport process is highly unidirectional. In detail, upon increasing the pH from 2.8 to 10, the current recorded at -2 V is very small (0.36 μA) and stays nearly unchanged (**Figure 2c**). At pH 2.8, the opening of the P4VP gates will allow the Cl^- inside the cavity to move out. Increasing the pH to 10.0 will open the PAA gate and the K^+ inside the cavity will move out. Similar phenomenon is also observed when we change the pH value reversely from 10 to 2.8 (**Figure 2d**). In both case, no enrichment and release of K^+ or Cl^- occurs, hence there is no net transmembrane transport of K^+ or Cl^-. The measured ionic current is very low and independent of pH variation.

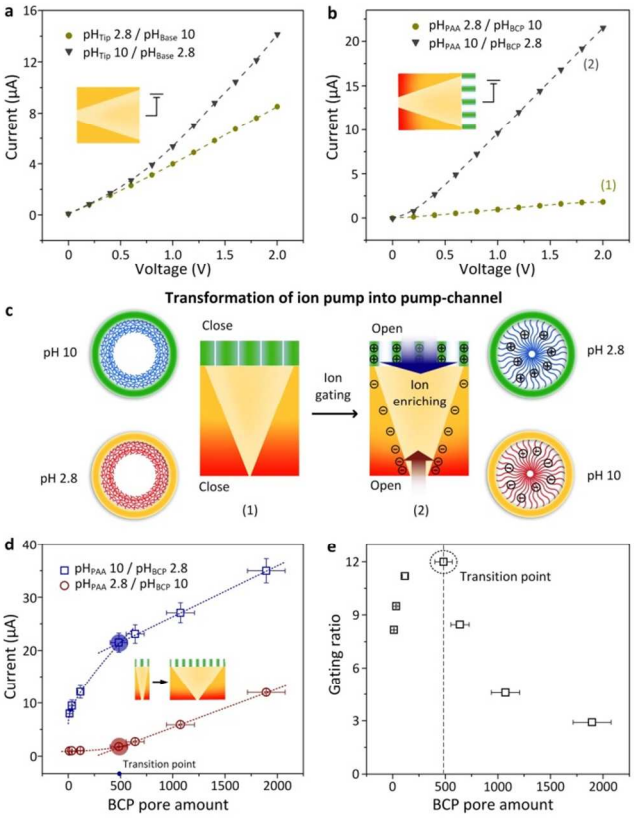

Figure 3. Pump–channel with controllable gating property. (a, b) *I-V* curves of the naked PET membrane with base approximately 1 μm in diameter (a) and the heterogeneous membrane (b) in 0.1 M KCl under asymmetric pH conditions. (c) Mechanism of the pump-channel feature. The two gates open or close simultaneously to ensure high-performance ion gating effect. (d, e) Effect of the pore amount of BCP membrane facing the base of PET membrane on the current at 2 V under different pH conditions (d) and the whole ion gating behavior (e).

The heterogeneous membrane can also function like ion channel mimicking biological pump–channels such as Na^+/ K^+ ATPase,[53] in which the ionic currents alternated between high and low conduction states by simultaneously opening or closing two polymer gates through exerting asymmetric pH 2.8/ 10 and 10/ 2.8 stimuli. **Figure 3a** shows the *I-V* curves of the naked PET membrane with base approximately 1 μm in diameter recorded in asymmetric pH condition, which exhibits poor gating behavior. When the alkaline solution is placed at the tip, the current is a little larger as the conical nanochannels are partially charged at tip.[54] After the heterogeneous system is formed, the current recorded at 2 V decreases to 1.8 μA (**Figure 3b**) under asymmetric pH 2.8/ 10 condition in which the PAA brushes and P4VP chains inside the pores of BCP membrane are both in collapsed, noncharged, and hydrophobic state (closed state). The system is in the closed state and the transmembrane ion transport is blocked, resulting in a very low ion current. On the contrary, under asymmetric pH 10/ 2.8 condition, both polymer gates would transform into swollen, charged, and hydrophilic state (open state). The system is in the open state and the ions could quickly flow from one side to the other side (**Figure 3c**, 2), contributing to a high ion current approximately 21.5 μA. The switching of these two asymmetric pH conditions caused the heterogeneous membrane exhibits high-performance ion gating behavior. Furthermore, the pump–channel and alternating gates ion pump can be switched with high stability (Figure S9).

The ion gating behavior is highly controllable due to the feasibility and accuracy in tuning the diameter of the bases of the PET nanochannels, which will change the exposed pore amount of BCP membrane facing the base of PET membrane.[42] As the pore amount increases, the current at 2 V under the two pH conditions both increases accordingly due to the decreasing transmembrane resistance (**Figure 3d**). Notably, the current increase is not linear, which is interpreted to be the cooperative effect of the PAA brushes at tip and the BCP membrane at base. Particularly, under pH 2.8/ 10, the rate of current rise increases as the pore amount increases from approximately 11 to 483, evidenced by an increasing slope. Next, continuously increasing the pore amount will result in a linear current increase. As the pore amount increases, the cone angle of PET nanochannel increases accordingly, resulting in a reduced effective sensing zone at the tip where PAA brushes locate in.[55,56] The hydrophobic effect of PAA brushes will weaken and thus the rate of current rise will increase at the initial stage. Continuously increasing the pore amount will further weaken the hydrophobic effect of PAA brushes, which will ultimately contribute to the subsequent linear current response. Similarly, under pH 10/ 2.8, the decreasing rate of current rise in the initial stage is caused by the gradual weakening of the hydrophilic effect at the tip upon pore amount increasing. On the whole, the ion gating ratio achieves a maximum value approximately 12 around the transition point (**Figure 3e**).

When the biological system such as CLC-ec1[57] is performing alternating gates ion pump functions, if one gate starts to open before the other gate closed completely, the system would function like a pump–channel operated in the open state. As such a breakdown would be so catastrophic; the biological ion pumps have evolved a fail-safe ion transport mechanism in which both gates first close, occluding the chosen ions inside the pore cavity, before the second gate opens to release them. Our heterogeneous system can also reproduced this fail-safe ion pump processes by integrating symmetric pH stimuli with asymmetric pH 10/ 2.8 conditions. In the experiments, the heterogeneous membrane is first placed in symmetric 2.8/ 2.8 condition; the P4VP gate inside the BCP membrane is opened to allow the entry of Cl^- from the base and the PAA gate is closed to block the ion transport at the tip, inducing a low ion current state (~2.30 μA at 2 V, **Figure 4**, 1). Then the P4VP gate inside the BCP membrane is closed by changing the pH on its side to 10, timely occluding the large amounts of Cl^- inside the channel cavity, which will result in a decreased ionic current (~1.86 μA at 2 V, **Figure 4**, 2). The PAA gate is subsequently opened by stimulating it with pH 10 to allow the ion exchange at the tip, releasing the accumulated Cl^- ions and contributing to a substantially increased ionic current (~8.34 μA at 2 V, **Figure 4**, 3). Finally, the PAA gate is closed by reducing the pH value on its side to 2.8; the K^+ ions are occluded in the nanochannel, resulting in a largely decreased ionic current (~1.85 μA at 2 V, **Figure 4**, 4).

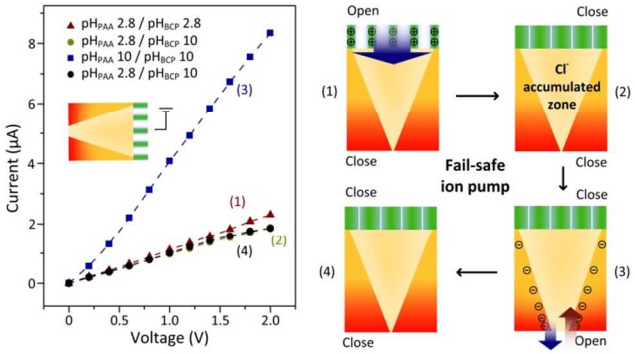

Figure 4. Fail-safe ion pump feature. *I-V* curves of the heterogeneous membrane in 0.1 M KCl when integrating symmetric pH stimuli with asymmetric pH 10/ 2.8 conditions, and the corresponding ion transport processes. The base of the PET channel is approximately 1 μm in diameter.

The biological alternating gates and fail-safe ion pumps can work well under both symmetric and asymmetric concentration environments. However, this is not case for the biological pump-channel as the fast ion transport can be strongly influenced by external concentration gradient.[24] Ionic transport properties of the heterogeneous ion pump system under symmetric and asymmetric concentration conditions are compared. As shown in **Figure 5a**, rational switching pH conditions of the two sides of the heterogeneous membrane under symmetric concentration environment (0.1 M/ 0.1 M) can contribute to three different ion transport processes. If we apply a concentration gradient (c_{PAA}/ c_{BCP}: 0.1 M/ 0.01 M) into the system,

significant enhancement and suppression of the ionic current is observed in the ion pump (i.e. alternating gates and fail-safe) and the pump–channel functions, respectively. The corresponding ion transport capability that calculated by averaging the ionic current of a whole ion transport process is shown in **Figure 5b**. Without a concentration gradient, the ion transport capability of alternating gates ion pump and fail-safe ion pump is much smaller than that of the pump–channel. This is because the migration of ions from one side to the other side through the nanochannel in these two functions must respectively undergo two and four ion transport states, leading to lower ion conduction, while this ion transmembrane transportation process in the pump–channel can be directly realized by its open state solely.[6,58] Under a concentration gradient, the ion transport capability of the bioinspired system increases both in the alternating gates ion pump and the fail-safe ion pump functions but reduces in the pump-channel function. These observations indicate that the artificial system can operate well both with and without a concentration gradient in the ion pump functions, but cannot operate well under a concentration gradient in the pump–channel function, which reproduced the ion transport phenomenon of biological systems.

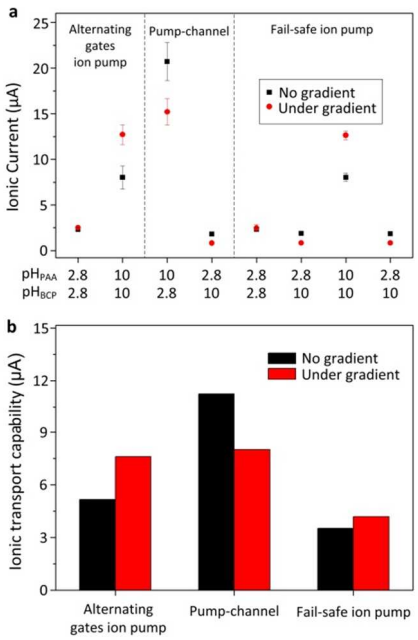

Figure 5. Effect of concentration gradient on the functions of three different ion transport processes. (a) Transmembrane ionic current measured at 2 V without (black) and under (red) a concentration gradient when we successively switching pH conditions of the two sides of the heterogeneous membrane. (b) Comparison of the ion transport capabilities of three ion transport processes without (black) and under (red) a concentration gradient. The base of the PET channel is also approximately 1 μm in diameter.

CONCLUSIONS

In summary, a bioinspired heterogeneous ion pump membrane is prepared by combining BCP coating and plasma grafting technique. Through activating the two polymers gates simultaneously or alternately, the hybrid membrane can well reproduce the three transport functions of the biological ion pump and can work well under a concentration gradient. The ion pumping function is highly selective to the anion and shows excellent unidirectionality. The PET channel with asymmetric geometry not only serves as a reserving space, but also introduces asymmetric ionic group distribution to the system, which is the key reason for this unidirectional ion pumping phenomenon. Furthermore, the gating function can be controlled with high precision through tuning the cooperative effect between the two separate gates by varying the size of the large opening of the PET membrane. This work extends our understanding of the biological ion pump and provides a framework for the design of asymmetric artificial ion pump system for the unidirectional transport of various types of cations, anions and molecules such as Na^+, Li^+, S^{2-} and protein, which would find applications in batteries, sensors, and desalination.[59-62]

EXPERIMENTAL SECTION

Chemicals: Polyethylene terephthalate membranes (PET, 12 μm thick) (GSI, Darmatadt, Germany). Potassium hydroxide (KOH), hydrogen chloride (HCl), potassium chloride (KCl), ethanol and dioxane were purchased from Sinopharm Chemical Reagent Beijing Co., Ltd. (SCRC, China) and J&K Beijing Co., Ltd. Acrylic acid (AAc) was purchased from Aladdin. Poly(styrene sulfonate) (PSS, M_w = 70 kg/mol) was purchased from Sigma-Aldrich. Polystyrene-*b*-poly(4-vinylpyridine) (PS-*b*-P4VP, M_n^{PS} = 48.4 kg/mol, M_n^{P4VP} = 21.3 kg/mol, PDI = 1.13), was purchased from Polymer Source. All solutions were prepared in MilliQ water (18.2 MΩ cm).

Plasma-Induced Graft Polymerization. Distilled AAc was placed in a monomer delivery system beforehand. The PET membrane with BCP membrane on the base was placed into the reaction chamber using a home-made mask that can expose the tip to the air. The loop of pumping and releasing argon gas in the reaction chamber ran three times. The vacuum before switching on the glow discharge was 16 Pa and the working temperature was 30 °C owing to the high volatility of AAc. Under the argon atmosphere about 50–60 Pa, a Start R-F power supply source was applied at 40 W to glow discharge and this process would last for 20 min. After the glow extinguished, grafting of the AAc monomers would take place in the reaction chamber, where a vacuum degree of 50–70 Pa was maintained. It would last about 20 min for the grafting reaction. After that, the chamber was connected to air. The plasma treatment was finished.

Electrical Measurements. The ionic transport properties of the system were examined by current-voltage

measurements using an electrochemical system at room temperature (≈ 23 °C). The separate PET membrane or the heterogeneous membrane was mounted between the two chambers of a custom-made electrochemical cell (Figure S7). The testing membrane area was about 0.12 cm^2. KCl was selected as the electrolyte as K^+ and Cl^- had a similar ion transference number and was injected into each chamber. 1 M HCl/ KOH were used to adjust the pH of the electrolyte solution to a desired value, and the influence of addition substance quality can be ignored. In this study, symmetric and asymmetric pH stimuli were adopted to regulate the charge and wettability of the two responsive polymers by adjusting pH values of solutions in the two chambers of the cell. Home-made Ag/AgCl electrodes were used to apply a transmembrane electrical potential and remained stable during the current recording process.

ASSOCIATED CONTENT

Supporting Information

Experimental procedures and additional figures. This material is available free of charge via the Internet at http://pubs.acs.org.

AUTHOR INFORMATION

Corresponding Author

tianyely@iccas.ac.cn;

wen@mail.ipc.ac.cn;

Notes

The authors declare no competing financial interest.

ACKNOWLEDGMENT

We thank the Material Science Group of Gesellschaft für Schwerionenforschung (Darmstadt, Germany) for providing the ion-irradiated samples. This work was supported by the National Key R&D Program of China (2017YFA0206904, 2017YFA0206900, 2017YFA0204504), the National Natural Science Foundation (21722309, 21671194, 21625303, 51673206, 21434003, 91427303), and the Key Research Program of the Chinese Academy of Sciences (KJZD-EW-M03, QYZDY-SSW-SLH014).

REFERENCES

(1) Xu, J.; Lavan, D. A. *Nat. Nanotechnol.* **2008**, *3*, 666.
(2) Clausen, T. *J. Gen. Physiol.* **2008**, *131*, 473.
(3) Gouaux, E.; MacKinnon, R. *Science* **2005**, *310*, 1461.
(4) White, R. J.; Ervin, E. N.; Yang, T.; Chen, X.; Daniel, S.; Cremer, P. S.; White, H. S. *J. Am. Chem. Soc.* **2007**, *129*, 11766.
(5) Zhang, Z.; Kong, X. Y.; Xie, G.; Li, P.; Xiao, K.; Wen, L. P.; Jiang, L. *Sci. Adv.* **2016**, *2*, e1600689.
(6) Gadsby, D. C. *Nat. Rev. Mol. Cell. Biol.* **2009**, *10*, 344.
(7) Shigekawa, M.; Iwamoto, T. *Circ. Res.* **2001**, *88*, 864.
(8) Artigas, P.; Gadsby, D. C. *Proc. Natl. Acad. Sci. U. S. A* **2003**, *100*, 501.
(9) Møller, J. V.; Nissen, P.; Sørensen, T. L.; le Maire, M. *Curr. Opin. Struct. Biol.* **2005**, *15*, 387.
(10) Gadsby, D. C.; Takeuchi, A.; Artigas, P.; Reyes, N. *Philos. Trans. R. Soc. Lond. B Biol. Sci.* **2009**, *364*, 229.
(11) Jardetzky, O. *Nature* **1966**, *211*, 969.
(12) Koltonow, A. R.; Huang, J. *Science* **2016**, *351*, 1395.
(13) Pérez-Mitta, G.; Marmisollé, W. A.; Trautmann, C.; Toimil-Molares, M. E.; Azzaroni, O. *J. Am. Chem. Soc.* **2015**, *137*, 15382.
(14) Dekker, C. *Nat. Nanotechnol.* **2007**, *2*, 209.
(15) Hou, X. *Adv. Mater.* **2016**, *28*, 7049.
(16) Cheng, C.; Jiang, G.; Garvey, C. J.; Wang, Y.; Simon, G. P.; Liu , J. Z.; Li, D. *Sci. Adv.* **2016**, *2*, e1501272.
(17) Buchsbaum, S. F.; Nguyen, G.; Howorka, S.; Siwy, Z. S. *J. Am. Chem. Soc.* **2014**, *136*, 9902.
(18) Madrid, E.; Rong, Y.; Carta, M.; McKeown, N. B.; Malpass-Evans, R.; Attard, G. A.; Clarke, T. J.; Taylor, S. H.; Long, Y. T.; Marken, F. *Angew. Chem., Int. Ed.* **2014**, *53*, 10751.
(19) Si, W.; Xin, P. Y.; Li, Z. T.; Hou, J. L. *Acc. Chem. Res.* **2015**, *48*, 1612.
(20) Ramirez, P.; Gomez, V.; Cervera, J.; Nasir, S.; Ali, M.; Ensinger, W.; Mafe, S. *Nano Energy* **2015**, *16*, 375.
(21) Afshar, M. G.; Crespo, G. A.; Bakker, E. *Angew. Chem. Int. Ed.* **2015**, *54*, 8110.
(22) Cervera, J.; Ramirez, P.; Mafe, S.; Stroeve, P. *Electrochim. Acta* **2011**, *56*, 4504.
(23) Siwy, Z. S.; Fuliński, A. *Am. J. Phys.* **2004**, *72*, 567.
(24) Zhang, H.; Hou, X.; Zeng, L.; Yang, F.; Li, L.; Yan, D.; Tian, Y.; Jiang, L. *J. Am. Chem. Soc.* **2013**, *135*, 16102.
(25) Su, B.; Tian, Y.; Jiang, L. *J. Am. Chem. Soc.* **2016**, *138*, 1727.
(26) Chen, L.; Si, W.; Zhang, L.; Tang, G. F.; Li, Z. T.; Hou, J. L. *J. Am. Chem. Soc.* **2013**, *135*, 2152.
(27) Zhang, J. C.; Yang, Y.; Zhang, Z. C.; Wang, P. P.; Wang, X. *Adv. Mater.* **2014**, *26*, 1071.
(28) He, D.; Madrid, E.; Aaronson, B. D.; Fan, L.; Doughty, J.; Mathwig, K.; Bond, A. M.; McKeown, N. B.; Marken, F. *ACS Appl. Mater. Interfaces* **2017**, *9*, 11272.
(29) Yang, H. C.; Hou, J.; Chen, V.; Xu, Z. K. *Angew. Chem., Int. Ed.* **2016**, 55, 13398.
(30) Wu, S. M.; Wildhaber, F.; Vazquez-Mena, O.; Bertsch, A.; Brugger, J.; Renaud, P. *Nanoscale* **2012**, *4*, 5718.
(31) Cheng, L. J.; Guo, L. J. *ACS Nano* **2009**, *3*, 575.
(32) Siria, A.; Poncharal, P.; Biance, A. L.; Fulcrand, R.; Blase, X.; Purcell, S. T.; Bocquet, L. *Nature* **2013**, *494*, 455.
(33) Ying, Y. L.; Zhang, J.; Gao, R.; Long, Y. T. *Angew. Chem., Int. Ed.* **2013**, 52, 13154.
(34) Hou, X.; Hu, Y.; Grinthal, A.; Khan, M.; Aizenberg, J. *Nature* **2015**, *519*, 70.
(35) Howorka, S.; Siwy, Z. *ACS Nano* **2016**, *10*, 9768.
(36) Feng, J.; Graf, M.; Liu, K.; Ovchinnikov, D.; Dumcenco, D.; Heiranian, M.; Nandigana, V.; Aluru, N. R.; Kis, A.; Radenovic, A. *Nature* **2016**, *536*, 197.
(37) Kim, D.; Duan, C.; Chen, Y.; Majumdar, A. *Microfluid. Nanofluid.* **2010**, *9*, 1215.
(38) Wang, Y.; Ou, R.; Wang, H.; Xu, T. *J. Membr. Sci.* **2015**, *475*, 281.
(39) Shao, J. J.; Raidongia, K.; Koltonow, A. R.; Huang, J. *Nat. Commun.* **2015**, *6*, 7602.
(40) Pérez-Mitta, G.; Tuninetti, J. S.; Knoll, W.; Trautmann, C.; Toimil-Molares, M. E.; Azzaroni, O. *J. Am. Chem. Soc.* **2015**, *137*, 6011.
(41) Ali, M.; Ahmed, I.; Nasir, S.; Ramirez, P.; Niemeyer, C.; Mafe, S.; Ensinger, W. *ACS Appl. Mater. Interfaces* **2015**, *7*, 19541.
(42) Scopece, P.; Baker, L. A.; Ugo, P.; Martin, C. R. *Nanotechnology* **2006**, *17*, 3951.
(43) Hou, X.; Zhang, H.; Jiang, L. *Angew. Chem., Int. Ed.* **2012**, *51*, 5296.
(44) Kim, S. H.; Misner, M. J.; Xu, T.; Kimura, M.; Russell, T. P. *Adv. Mater.* **2004**, *16*, 226.

(45) Schacher, F. H.; Rupar, P. A.; Manners, I. *Angew. Chem., Int. Ed.* **2012**, *51*, 7898.
(46) Nasir, S.; Ali, M.; Ramirez, P.; Gómez, V.; Oschmann, B.; Muench, F.; Tahir, M. N.; Zentel, R.; Mafe, S.; Ensinger, W. *ACS Appl. Mater. Interfaces* **2014**, *6*, 12486.
(47) Qiu, X. Y.; Yu, H. Z.; Karunakaran, M.; Pradeep, N.; Nunes, S. P.; Peinemann, K. V. *ACS Nano* **2013**, *7*, 768.
(48) Yameen, B.; Ali, M.; Neumann, R.; Ensinger, W.; Azzaroni, O. *Nano Lett.* **2009**, *9*, 2788.
(49) Zhang, Z.; Sui, X.; Li, P.; Xie, G.; Kong, X. Y.; Xiao, K.; Gao, L.; Wen, L.; Jiang, L. *J. Am. Chem. Soc.* **2017**, *139*, 8905.
(50) Gilles, F. M.; Tagliazucchi, M.; Azzaroni, O.; Szleifer, I. *J. Phys. Chem. C* **2016**, *120*, 4789.
(51) Sparreboom, W.; van den Berg, A.; Eijkel, J. C. *Nat. Nanotechnol.* **2009**, *4*, 713.
(52) Schoch, R. B.; Han, J.; Renaud, P. *Rev. Mod. Phys.* **2008**, *80*, 839.
(53) Artigas, P.; Gadsby, D. C. *Ann. NY Acad. Sci.* **2002**, *976*, 31.
(54) Lan, W. J.; Edwards, M. A.; Luo, L.; Perera, R. T.; Wu, X.; Martin, C. R.; White, H. S. *Acc. Chem. Res.* **2016**, *49*, 2605.
(55) Daiguji, H. *Chem. Soc. Rev.* **2010**, *39*, 901.
(56) Harrell, C. C.; Siwy, Z. S.; Martin, C. R. *Small* **2006**, *2*, 194.
(57) Accardi, A.; Miller, C. *Nature* **2004**, *427*, 803.
(58) Gadsby, D. C. *Nature* **2004**, *427*, 795.
(59) Yusko, E. C.; Bruhn, B. R.; Eggenberger, O. M.; Houghtaling, J.; Rollings, R. C.; Walsh, N. C.; Nandivada, S.; Pindrus, M.; Hall, A. R.; Sept, D.; Li, J.; Kalonia, D. S.; Mayer, M. *Nat. Nanotechnol.* **2017**, *12*, 360.
(60) Abraham, J.; Vasu, K. S.; Williams, C. D.; Gopinadhan, K.; Su, Y.; Cherian, C. T.; Dix, J.; Prestat, E.; Haigh, S. J.; Grigorieva, I. V.; Carbone, P.; Geim, A. K.; Nair, R. R. *Nat. Nanotechnol.* **2017**, *12*, 546.
(61) Howorka, S. *Nat. Nanotechnol.* **2017**, *12*, 619.
(62) Chen, Y.; Yu, X.; Li, Z.; Paik, U.; Lou, X. W. *Sci. Adv.* **2016**, *2*, e1600021.

SYNOPSIS TOC